Available online at www.sciencedirect.com
SCIENCE DIRECT®
Journal of Solid State Chemistry 178 (2005) 142–152
JOURNAL OF SOLID STATE CHEMISTRY
www.elsevier.com/locate/jssc

Structural and thermal properties of Co–Cu–Fe hydrotalcite-like compounds

Amadeu H. Iglesias[a], Odair P. Ferreira[a,*], Daniel X. Gouveia[b,c], Antonio G. Souza Filho[b], José A.C. de Paiva[b], Josué Mendes Filho[b], Oswaldo L. Alves[a]

[a]*LQES–Laboratório de Química do Estado Sólido, Instituto de Química, State University of Campinas (UNICAMP), P.O. Box 6154, zip code 13081-970, Campinas, SP, Brazil*
[b]*Departamento de Física, Universidade Federal do Ceará, P.O. Box 6030, zip code 60455-900, Fortaleza, CE, Brazil*
[c]*Centro Federal de Educação Tecnológica-CEFET, zip code 60040-531, Fortaleza,CE, Brazil*

Received 25 August 2004; received in revised form 18 October 2004; accepted 29 October 2004

Abstract

The structural properties and thermal decomposition processes of Co–Cu–Fe ternary hydrotalcites (HT) have been studied through X-ray diffraction, thermogravimetric measurements, Fourier-transform infrared and Mössbauer spectroscopies. Due to the strong Jahn–Teller effect, the Cu–Fe layered system is stabilized only in the presence of Co^{2+}. At low Co^{2+} contents, additional phases are segregated in the solids. X-ray patterns show the presence of $Cu(OH)_2$ and CuO. The decomposition process was investigated by in situ X-ray, in situ Mössbauer and FTIR experiments. By increasing the temperature from 25 °C up to 180 °C we observed that the structural disorder increases. This effect has been likely attributed to the $Co^{2+} \rightarrow Co^{3+}$ oxidation since thermal decomposition was carried out under static air atmosphere. Part of the Co^{3+} cations could migrate to the interlayer region, thus forming a metastable compound that still has a layered structure. Collapse of the layered structure was observed at about 200 °C. By further increasing the temperature the system becomes more crystalline and the formation of Co_3O_4 is observed in the X-ray patterns. In Cu-rich HT, some of the carbonate anions are released at temperatures higher than 550 °C and this phenomenon is attributed to the formation of a carbonate-rich phase. The specific surface area data present its highest values in the temperature range where the collapse of the layered structure takes place.

Keywords: Layered double hydroxides; Hydrotalcite-like compounds; Anionic clays; Thermal decomposition; Mixed oxides; ^{57}Fe Mössbauer spectroscopy; Decomposition mechanism; Copper

1. Introduction

Layered double hydroxides, also known as hydrotalcite-like compounds or simply hydrotalcites (HT) are bidimensional layered materials with the general formula $[M^{2+}_{1-x}M^{3+}_{x}(OH)_2]^{x+}(A^{n-}_{x/n})^{x-}\cdot mH_2O$, where M^{2+} is a divalent cation (Mg^{2+}, Co^{2+}, Ni^{2+}, Zn^{2+}, Mn^{2+}, Cd^{2+}), M^{3+} is a trivalent cation (Al^{3+}, Fe^{3+}, Cr^{3+}, Ga^{3+}) and A^{n-} is an anion [1–6]. These solids present a brucite-like structure, where metallic cations are located in the center of an edge-sharing octahedral network. Isomorphous substitution of divalent cations by trivalent ones generates positive charges on the layers, which are compensated by anions located in the interlayer region. Water molecules are also found in the interlayer space. Both anions and water molecules are arranged in a liquid-like configuration (for a schematic view of hydrotalcite structure see Ref. [1]) [1–4].

HT have received considerable attention in recent decades due to their potential applications in many

*Corresponding authors. Tel.: +55 19 3788 3394; fax: +55 19 3788 3023.
E-mail addresses: odair@iqm.unicamp.br (O.P. Ferreira), oalves@iqm.unicamp.br (O.L. Alves).
URL: http://lqes.iqm.unicamp.br.

0022-4596/$ - see front matter © 2004 Elsevier Inc. All rights reserved.
doi:10.1016/j.jssc.2004.10.039

different fields, such as ion exchangers, adsorbents, medical science and catalysts [7–12]. This wide range of applications comes from some special features of the HT structure, as follows: possibility of accommodation of cations of different natures in the sheets, atomic scale homogeneity, possibility of intercalation of several types of anions (inorganic, organic, organometallic, polyoxometalates) and formation of mixed oxides under thermal treatment [3,5]. This last feature is very important because, by choosing the appropriate decomposition atmosphere, the nature of the oxide phase can be controlled [13,14]. It is also known that HT containing transition metals tend to exhibit enhanced catalytic activity owing to the presence of redox and Lewis sites that may be combined with structural and geometric features to yield solids with the desired properties [15].

The interest in modifying Co–Fe-based HT as a function of Cu^{2+} addition and understanding its thermal decomposition step-by-step comes from the fact that these modified systems and the oxides resulting from their thermal decomposition process are suitable for applications in heterogeneous catalysis when combined with oxi-reduction reactions. Copper-based HT and their decomposition products are known to be active catalysts for oxidation reactions [16–18]. Cobalt-based HT or the oxides obtained after thermal treatment are being continuously developed for their use in the Fischer-Tropsch process [19,20] and steam-reforming [21]. Furthermore, HT containing these metals (Co or Cu) have also found important environmental applications, such as in the removal or decomposition of SO_x and NO_x [22–24].

Several studies have been performed in order to evaluate structural changes during thermal treatment of HT, although few of them make use of in situ techniques [13,14,25–31]. The use of such techniques is of great importance in the study of the thermal decomposition, since cooling, the exposure to atmosphere and handling can lead to important structural changes. Among the in situ techniques used, the most common are XRD, FTIR and Raman spectroscopy [14,27,30]. Moreover, techniques using atomic probing are necessary in order to obtain precise information about the decomposition pathway, since intermediate compounds formed during the process lack long-range order. In this scenario, ^{27}Al MAS NMR and XAS spectroscopy have been the most used techniques [25,29]. Consequently, the use of a technique such as in situ Mössbauer spectroscopy, which combines both advantages mentioned above, can lead to an enormous gain in the understanding of the processes involved in the changes occurring in the lamellar structure of the material during the heating process.

This work reports the synthesis and characterization of ternary $(Co_{1-y}Cu_y)_{1-x}Fe_x(OH)_2(CO_3)_{x/2}\cdot mH_2O$ HT compounds and their thermal decomposition behavior by using short and long-range order techniques. The main focus relies on the investigation of structural and thermal effects of Cu^{2+} addition to Co–Fe-based HT, aiming to understand the system in order to make rational use of these modified HT and enhance their applications. To the best of our knowledge, this kind of study has not yet been reported for a ternary HT containing only transition metals. Furthermore, the small step used in the temperature dependent measurements is another characteristic issue of the present work that allowed us to monitor the decomposition process in depth.

2. Experimental procedure

2.1. Materials

The starting materials (reagent grade and used as received) for preparing the ternary HT were $Co(NO_3)_2\cdot 6H_2O$ (Vetec), $Cu(NO_3)_2\cdot 3H_2O$ (Synth), $Fe(NO_3)_3\cdot 9H_2O$ (Vetec), Na_2CO_3 (Synth) and NaOH (Synth). All solutions were prepared with deionized water.

2.2. Preparation of hydrotalcites

The layered double hydroxides with molar ratio $(Co^{2+}+Cu^{2+})/Fe^{3+}=2$ were prepared by using the co-precipitation method at variable pH. 200 mL of an aqueous solution containing Co^{2+}, Cu^{2+} and Fe^{3+} (the relation $Co^{2+}+Cu^{2+}=0.06$ mol was kept constant) was slowly added dropwise under vigorous mechanical stirring into 200 mL of another solution containing 1.0 mol L^{-1} NaOH and 0.30 mol L^{-1} Na_2CO_3. The samples obtained with $Cu^{2+}/(Cu^{2+}+Co^{2+})$ molar contents of 0, 10%, 30%, 50% and 100% were submitted to an ageing treatment at 60 °C for 40 h. The pH of the mother liquor after the ageing process varied from 10.0 to 11.0. The prepared solids were isolated by filtration and washed several times with deionized water until the pH reached 7.0. Afterwards the solids were dried at 60 °C for 24 h. The samples are labeled HTCu followed by the respective nominal Cu content relative to $(Co^{2+}+Cu^{2+})$. Thus, HTCu30 stands for a sample with Cu concentration of 30% of the $Co^{2+}+Cu^{2+}$ concentration.

2.3. Techniques

Chemical analysis for Co, Cu and Fe were carried out by inductively coupled plasma optical emission spectrometry (ICPOES), using a Perkin-Elmer, model Optima 3000 DV, after dissolution of the sample in 0.1 mol L^{-1} HCl.

In order to evaluate the presence of oxidized Co (Co^{3+}) in the samples, the redox titration method described by Zeng et al. was used [32]. Approximately 10 mg of each sample was dissolved in 20 mL of 1.0 mol L^{-1} HCl solution with gentle heating. A nitrogen flow was used to purge a solution containing 50 mL of 0.01 mol L^{-1} KI and starch indicator.

Powder X-ray diffraction (XRD) patterns were obtained with a Shimadzu XRD6000 diffractometer, using Cu$K\alpha$ ($\lambda = 1.5406$ Å) radiation operating with 30 mA and 40 kV. A scan rate of 1° min^{-1} was employed. In order to determine accurately the cell parameter a, scans were made in the 58–62° 2θ region using a scan rate of 0.1° min^{-1}. In situ XRD measurements were carried out in the 25–400 °C temperature range by using a high temperature furnace (HA1001, Shimadzu). The heating rate was 5.0 °C min^{-1} and before each measurement a time interval of 20 min was used for stabilizing the temperature.

The Fourier transform infrared spectroscopy (FTIR) spectra were recorded using the KBr pellet technique on a Bomem MB spectrometer in the 4000–400 cm^{-1} wavenumber range. The pellets were prepared by weighing approximately 100 mg of KBr and 1 mg of the sample in order to avoid mass/concentration effects on the spectra. A total of 16 scans and a resolution of 4 cm^{-1} were employed to obtain the spectra. Spectra recorded in the 450–250 cm^{-1} range were collected in the same equipment using the Fluorolube emulsion technique and a polyethylene window. In order to have a FTIR assessment of thermal decomposition, the samples were calcined using a Thermolyne F21100 Tube Furnace with a heating rate of 5 °C min^{-1} and kept at each temperature for 1 h. After that, samples were cooled to room temperature in a desiccator and the spectra were collected using the Fluorolube emulsion technique (KBr window) in the spectral range of 1550–1300 cm^{-1}.

The Mössbauer measurements were performed at room temperature on powdered samples by using standard transmission geometry and a constant acceleration spectrometer with a radioactive source of ^{57}Co within an Rh host. The spectra analyses were performed by using the Normos fitting routine which makes use of a Lorentzian set and computes the contribution of each curve to the total absorption spectrum through the least-squares procedure. All the isomer shifts (δ) quoted in this paper are relative to metallic iron (α-Fe). We have used a home made Mössbauer furnace, coupled to a ± 2 °C temperature controller (Eurotherm). The samples were held for approximately 20 min for stabilization at the desired temperature before each measurement.

Thermogravimetric (TGA) analysis were carried out using a TA Instruments 500 TGA 2050 in the 25–700 °C temperature range with a heating rate of 5 °C min^{-1} under an air flow of 100 mL min^{-1}.

The differential thermal analysis (DTA) experiments were performed using a Shimadzu instrument (model 50 WS) in the 25–650 °C temperature range. The measurements were carried out under an air flow of 100 mL min^{-1} and with a heating rate of 5 °C min^{-1}.

Specific surface area measurements were determined by nitrogen adsorption–desorption in a Flowsorb 2300 (Micrometrics Instrument Corp.), using the BET method.

3. Results and discussion

3.1. Characterization of the hydrotalcites

3.1.1. Elemental chemical analysis

The results of chemical analysis are shown in Table 1. The Cu^{2+}/Co^{2+} and M^{2+}/Fe^{3+} molar ratios observed for the precipitated solids are very close to the nominal ratios used for preparing the starting solutions, thus showing that the precipitation process was efficient.

The chemical formulae calculated for the HT samples are in Table 2. HTCu50 and HTCu100 samples do not exhibit a single HT phase, as discussed later in the XRD results. The content of carbonate anions has been calculated from the M^{2+}/Fe^{3+} ratio by considering that no $Co^{2+} \rightarrow Co^{3+}$ oxidation has occurred (as indicated by the chemical titration for all the samples), and assuming that carbonate is the main interlayer anion (this is supported by FTIR results to be discussed later) responsible to balance the positively charged brucite-like sheets. The water content was evaluated from the TGA results.

3.1.2. X-ray powder diffraction

The X-ray diffractograms of the synthesized samples are shown in Fig. 1. The samples HTCu0, HTCu10, HTCu30 and HTCu50 exhibit the typical signature of a crystalline layered double hydroxide belonging to the space group $R\bar{3}m$ (JCPDS card 25–0521) [33,34]. Neither secondary phases nor changes in the baseline of the diffractograms are observed for HTCu0, HTCu10 and HTCu30 thus indicating that these HT exhibit a single crystalline phase. This is not the case for the HTCu50 sample where impurity peaks (marked with + in Fig. 1) were indexed to a $Cu(OH)_2$ phase (space group *Cmcm*, JCPDS card 13–0420). When the precipitation is performed in the absence of Co^{2+} there is no formation of the Cu–Fe layered double hydroxide using our experimental conditions and synthesis method. In the HTCu100 X-ray pattern we could identify the presence of the CuO tenorite phase (space group $C2/c$, JCPDS card 05–0661). Such a diffractogram also presents changes in the baseline through the rising of a broad background thus indicating the formation of an amorphous phase that may be related to some Fe

Table 1
Elemental chemical analysis results for the as prepared HT samples

Sample	Co[a]	Cu[a]	Fe[a]	Cu/Co[b]		M^{2+}/Fe[b]	
				Solution	Solid	Solution	Solid
HTCu0	33.0	—	16.6	—	—	1.999	1.900
HTCu10	33.2	4.5	18.2	0.111	0.126	1.998	1.950
HTCu30	26.4	13.3	18.6	0.429	0.467	2.003	1.970
HTCu50	18.9	21.8	18.3	0.999	1.070	1.999	2.030
HTCu100	—	47.6	20.6	—	—	2.000	2.030

[a]Weight percent.
[b]Molar ratio.

Table 2
Chemical formulae calculated for the as prepared HT samples

Sample	Formulae	c (Å)	a (Å)
HTCu0	$Co_{0.66}Fe_{0.34}(OH)_2(CO_3)_{0.17}\cdot 0.34H_2O$	22.77	3.120
HTCu10	$Co_{0.58}Cu_{0.08}Fe_{0.34}(OH)_2(CO_3)_{0.17}\cdot 0.23H_2O$	22.79	3.118
HTCu30	$Co_{0.45}Cu_{0.21}Fe_{0.34}(OH)_2(CO_3)_{0.17}\cdot 0.13H_2O$	22.77	3.117
HTCu50	$HT + Cu(OH)_2$	22.69	3.117
HTCu100	There is no HT phase formation.		

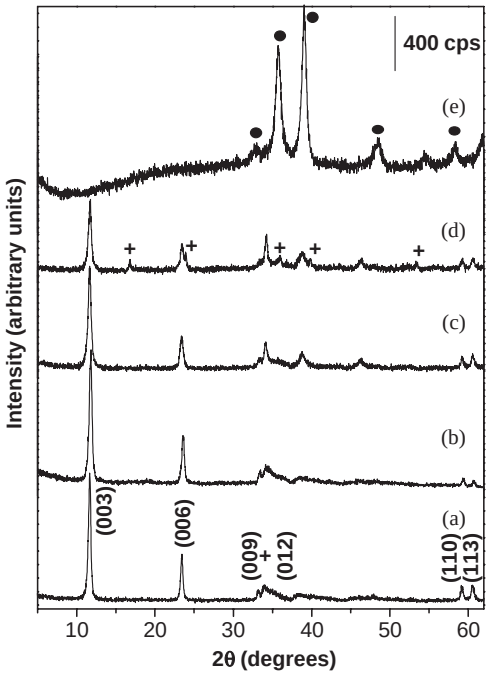

Fig. 1. XRD patterns of Co–Cu–Fe-based HT as a function of Cu concentration. (a) HTCu0; (b) HTCu10, (c) HTCu30, (d) HTCu50, (e) HTCu100. (+) and (●) stand for $Cu(OH)_2$ and CuO phases, respectively.

compound, as revealed by Mössbauer measurements discussed later. It is well-known that $Cu(OH)_2$ is very unstable in highly basic media and can be easily transformed into CuO [35]. This suggests that the CuO detected in the HTCu100 sample comes from $Cu(OH)_2$ formed in the precipitation step that was transformed into CuO during the ageing treatment. Therefore, the presence of Co^{2+} is fundamental for preparing the Cu–Fe HT phase when using the synthesis route described in the experimental section.

The a and c cell parameters calculated from X-ray data are listed in Table 2. The c parameter corresponds to three times the interlayer distance $d_{(003)}$ that is obtained from the (003) diffraction peak. The a cell parameter stands for the cation–cation average distance inside the layers and can be determined from the angular position of the (110) reflection. The values observed for the c parameter are typical of HT containing carbonate as the interlamellar anion [1,2,36]. It has been reported [1,36] that the interlayer distance depends on the size and the orientation of the interlayer anions as well as on the thickness and charge density of the layers. The layer thickness strongly depends on the size of the cations and it is almost the same for the first row of transition metals. It turns out that, as the charge density increases, the parameter c decreases because there is an increment of the Coulomb forces (attractive) between the positive (layers) and negative (interlamellar region) charged regions [36]. It can be observed from Table 2 that parameter c is practically constant for the samples HTCu0, HTCu10 and HTCu30 and slightly decreases for sample HTCu50. The slight decrease in the c parameter for the HTCu50 sample suggests that segregation of a Cu-rich phase (identified as $Cu(OH)_2$) has occurred, thus increasing the charge density in the

layers which leads to an increase in the attractive electrostatic force, contracting the layer distance.

HT containing different Cu concentrations present very close values for the a parameter (see Table 2). A similar result has been reported by Leroux et al. [37] for the $(Co_{1-y}Cu_y)_2Al(OH)_6Cl \cdot nH_2O$ system. This is reasonable since Co^{2+} and Cu^{2+} have very similar ionic radius. The increase of Cu^{2+} concentration leads to a broadening of the (110) diffraction peak, thus indicating that the layers are becoming more disordered.

In general, the synthesis of single HT phases containing Cu^{2+} as divalent metal is somewhat difficult and a second divalent metal with different nature has been used to stabilize Cu-based HT. It is well known that in octahedrally coordinated complexes the Cu^{2+} (d^9 configuration) exhibits a strong Jahn–Teller effect. It is most likely that, for low Cu^{2+} content, the distortion introduced in the brucite-like layers due to the presence of copper can be accommodated in the crystalline lattice. However, when the Cu^{2+} content is high, the crystalline lattice cannot accommodate such distortions as discussed by Vaccari et al. [1]. For Cu^{2+}/M^{II} ratios smaller than 1 the Cu^{2+} cations are well separated from each other and they are arranged in a typical octahedral network. When the Cu^{2+}/M^{II} ratio is higher than 1 the Cu^{2+} ions are distributed in neighbor octahedra and the formation of Cu compounds is energetically favored over the HT structure. Consequently, the formation of $Cu(OH)_2$ phase in the HTCu50 sample and the inhibition of HT formation for the HTCu100 sample is fundamentally linked to the Jahn–Teller effect.

3.1.3. FTIR spectroscopy

The FTIR spectra of the as prepared samples are shown in Fig. 2 and they are typical of HT compounds containing mainly CO_3^{2-}, except for the HTCu100 sample that does not form the HT phase.

The broad band observed at about 3420 cm^{-1} is assigned to O–H stretching (ν_{O-H}) due to the presence of hydroxyl as well as both adsorbed and interlayer water. The shoulder observed at 3040 cm^{-1} (marked with an up arrow) can be assigned to hydrogen bonds between water and CO_3^{2-} [39]. This mode is not observed for HTCu100 where the HT phase is not formed. The bending mode H–O–H from H_2O was observed at 1640 cm^{-1} thus confirming the presence of water in the interlayer space. The presence of a narrow mode (marked with a solid circle) for the HTCu50 sample is remarkable. This mode has been assigned to the O–H stretching of free metallic hydroxide in agreement with the X-ray results where we observed the presence of $Cu(OH)_2$ in this sample. Finally, there is a drastic decrease in the intensity of the O–H related modes for sample HTCu100, thus indicating only a small amount of hydroxyl groups. This is in very good agreement with the X-ray results that indicated the presence of CuO rather than the Cu–Fe HT phase.

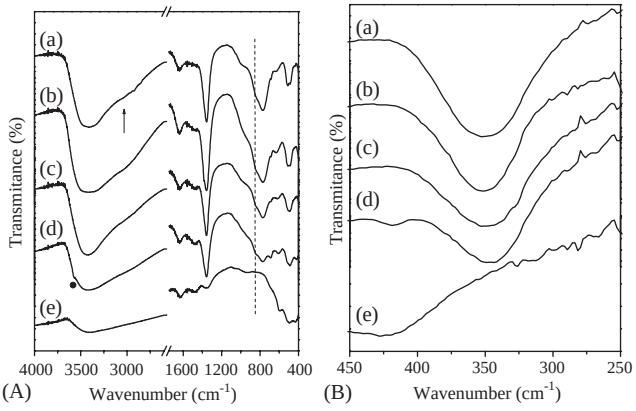

Fig. 2. FTIR spectra in the 4000–400 cm^{-1} (A) and 450–250 cm^{-1} (B) range for the as prepared samples: (a) HTCu0; (b) HTCu10; (c) HTCu30; (d) HTCu50; and (e) HTCu100.

The sharp band observed at about 1360 cm^{-1} (traces a–d in Fig. 2A) in the FTIR spectra is attributed to the ν_3 asymmetric stretching of the CO_3^{2-}. The position of this mode does not depend on Cu content in the brucite-like layers. When compared with free CO_3^{2-} ($\nu_3 = 1415\ cm^{-1}$) [40], the ν_3 mode observed in HT appears downshifted by 55 cm^{-1} due to interaction of these anions with water molecules through hydrogen bonds. However, these interactions are not strong enough to distort the CO_3^{2-} anions from their D_{3h} free molecule symmetry. The shoulder observed at 840 cm^{-1} (marked with a dashed line) is assigned to the ν_2 bending mode of the carbonate anion. Its intensity is drastically reduced for the HTCu100 sample (lower trace in Fig. 2A) where there is no formation of HT phase.

The IR modes below 800 cm^{-1} can be attributed to the M–OH (traces a–d in Fig. 2A) and M–O (traces a–d in Fig. 2B) vibrations. The broad band centered at 770 cm^{-1} is assigned to the $\delta(M\text{OH})$ mode whereas the mode observed in the 250–400 cm^{-1} spectral region can be assigned to stretching $\nu(M\text{–O})$ [31,33,34]. Since Co, Cu and Fe have very close mass values, the Cu content does not significantly affect the energy of the M–O vibrations. In fact, Cu–O, Co–O and Fe–O vibration frequencies are very close, thus giving rise to a broad band. It was observed that their intensity decreases as the Cu content increases. This band at 350 cm^{-1} is a signature of the HT phase and it disappears for the HTCu100 sample where a new mode at 425 cm^{-1} appears in the spectra attributed to copper oxide and/or iron oxyhydroxides [41].

3.1.4. Mössbauer spectroscopy

Mössbauer spectra and parameters obtained for ternary HT with varying Cu content are shown in Figs. 3A and B, respectively.

The Isomer Shift and Quadrupole Splitting values indicate that the probe atom is in the Fe^{3+} oxidation

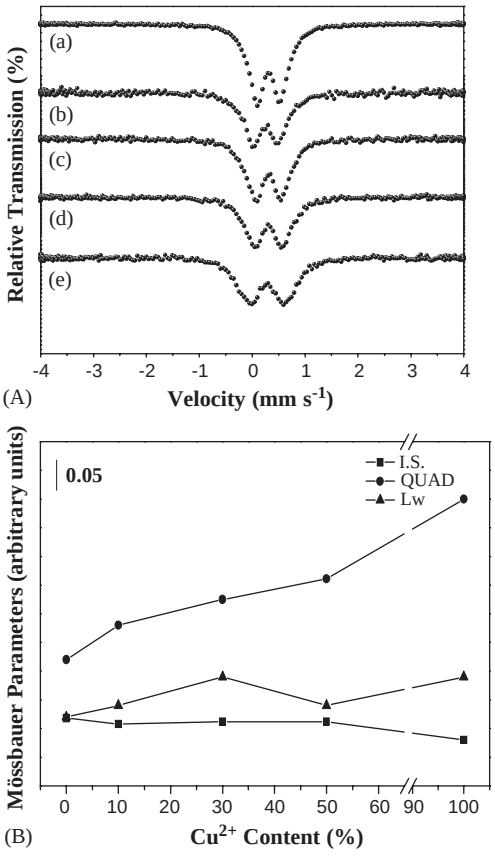

Fig. 3. (A) Mössbauer spectra for different Cu concentration taken at room temperature. (B) The Mössbauer parameters Isomer Shift (I.S.), Quadrupole Splitting (QUAD) and Linewidth (LW) as a function of Cu concentration. (a) HTCu0; (b) HTCu10; (c) HTCu30; (d) HTCu50; and (e) HTCu100.

state with octahedral coordination. Both Isomer Shift and Linewidth are nearly constant as the Cu content varies. However, the Quadrupolar Splitting values systematically increase as the Cu concentration increases. This result indicates that the replacement of Co by Cu induces some distortion in the Fe^{3+} coordination sphere. This can be further understood based on the electronegativity of the divalent species.

It is well-known that the covalent character of the chemical bond between ligands and the probe-atom contributes to the quadrupolar splitting values [42]. As the covalent bond becomes stronger the quadrupolar splitting becomes smaller. Co has an electronegativity of 1.8, less electronegative than Cu (1.9). So, when Co are replaced by Cu, the electronic density due to oxygen atoms are more attracted to the Cu atoms, thus decreasing the covalent character of the Fe–O bonds. This leads to a spatial distortion of the octahedral coordination proportional to Cu content that is reflected in the quadrupolar splitting values observed in Fig. 3B. This result further confirms that the Cu atoms are incorporated into the layers by occupying the Co positions, in agreement with the X-ray data. The quadrupolar splitting values for the HTCu100 sample exhibits the highest values of all the five samples. This high value of quadrupolar splitting indicates that, for this sample, the Fe^{3+} chemical environmental is more disordered than in the other samples. Thus, the amorphous phase observed in the X-ray diffraction for HTCu100 should be Fe-based oxides.

3.2. Thermal properties of Co–Cu–Fe hydrotalcites

We have studied the thermal behavior of Co–Cu–Fe HT by using DTA, TG, in situ X-ray diffraction, in situ ^{57}Fe Mössbauer spectroscopy and FTIR spectroscopy. Both in situ X-ray diffraction and in situ ^{57}Fe Mössbauer spectroscopy are, respectively, powerful tools for understanding and probing the structural properties at long-range and short-range order of the HT during thermal decomposition. In order to guide the in situ experiments we have first performed DTA and TG experiments.

3.2.1. DTA and TG analysis

The DTA and TG curves for the samples obtained are shown in Figs. 4A and B, respectively.

The DTA profiles are qualitatively similar for all the samples, differing only in the temperatures where the minimum occurs. Two endothermal peaks are observed: an intense (weak) peak located in the 150–170 °C (170–220 °C) temperature.

Both the temperature and the intensity of the first peak decreases as the Cu content increases, whereas for the second peak the temperature is independent of the Cu content for samples HTCu0, HTCu10 and HTCu30. However, for sample HTCu50, the second peak becomes broader and shifts to lower temperature (170 °C), which could be related to the presence of impurities. Rives et al. [15,38] showed that the first endothermic peak for the systems Cu–Co–Al and Cu–Ni–Al also present a shift towards lower temperatures with increasing Cu^{2+} in the brucite-like sheets. This behavior indicates that

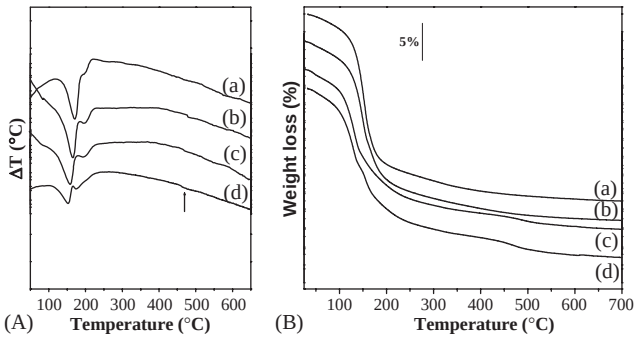

Fig. 4. DTA (A) and TG (B) curves for the HT with varying Cu contents. (a), (b), (c) and (d) indicate HTCu0, HTCu10, HTCu30, and HTCu50 samples, respectively.

for HT containing Cu^{2+} as a co-bivalent cation thermal stability decreases with increasing copper concentration. The fact that the second peak remains at the same temperature range indicates that it is due to the same reaction: elimination of hydroxil groups (as water molecules) and carbonate (as CO_2) [14,26]. In addition, the presence of Co^{2+} in the brucite layer leads to a reduction in the thermal stability of HT when compared with other systems owing to the possibility of oxidation of this cation [13]. Furthermore, there is a very weak endothermic peak in the DTA scans located at about 480 °C for Cu-rich samples (marked with an up arrow in Fig. 4A).

The TG scans are qualitatively the same for all the samples studied. A continuous weight loss is the most important event occurring in the 100–220 °C temperature range. The upper trace in Fig. 4B stands for TG scan of the HTCu0 sample. From 25 to 220 °C there is a 22% weight loss while from 220 to 600 °C the weight loss is only 4%. These weight losses can be attributed to the following thermal events: (i) release of both interlamellar and adsorbed water, keeping the layered structure; and (ii) release of hydroxyl groups from the brucite-like layers (as water) and the release of the interlamellar anion as CO_2 [14,26,30]. In this later process there is a collapse of the layered structure.

The HT containing Cu also present a continuous weight loss up to 600 °C and the principal thermal events are the same as discussed for the sample without Cu. A weight loss of 21–25% is observed, decreasing as the Cu content increases. For samples HTCu30 and HTCu50 a weight loss at about 480 °C is seen, occurring at the same temperature as the shoulder discussed in the DTA scans. This phenomenon observed for Cu-rich HT can be attributed to the formation of copper oxy-carbonate, like $Cu_xM_yO_z(CO_3)_m$, as discussed in the FTIR results [26,27].

3.2.2. *In situ X-ray diffraction*

In order to monitor the structural changes which Co–Cu–Fe HT underwent during thermal decomposition, in situ X-ray diffraction experiments were performed, whose results are shown in Fig. 5.

By observing the XRD patterns we can state that the thermal decomposition process is similar for the three samples. From 25 °C up to 140 °C the XRD curves do not exhibit any significant changes. The diffracted lines gradually lose intensity and become broader. However, the *a* and *c* parameters remain almost constant. In this temperature range, the TG scans indicate a weight loss of about 8–10% that, in principle, could be attributed to the removal of both adsorbed and interlamellar water along with the start of the decomposition of the brucite-like layers and the interlamellar anions [14]. It should be pointed out that the (003) peaks do not shift their angular position up to 140 °C. This result suggests that the water molecules occupy interstitial positions in the interlamellar space that are not occupied by CO_3^{2-}. This behavior was also observed by Petrova et al. [43] for the Mg–Al–CO_3 system that when thermally treated up to 160 °C, had no more interlamellar water although the c parameter did not change. This behavior can be related to the M^{2+}/M^{3+} molar ratio. This ratio becomes lower, the higher is the amount of anions in the interlamellar region and the environment for water molecules becomes more restricted thus implying that they will be more likely to occupy the interstitial sites.

At 160 °C the X-ray patterns show a drastic decrease of intensity of the (00*l*) reflections and do not exhibit (11*l*) reflections. The decrease in the intensity of the (00*l*) reflections indicates a disorder in the stacking of the layers. The (003) diffraction line becomes less intense and broader, developing an asymmetry at the higher 2θ. However, the occurrence of this diffraction line indicates only partial destruction of the layered structure. The asymmetry observed in this reflection is due to the contraction of the interlayer distance, which can be explained by one of the following mechanisms: (i) the grafting of the carbonate anions [44] or (ii) the migration of the Co^{3+} to the interlayer space [14]. According to our results (in situ DRX, FTIR and Mössbauer Spectroscopy), we believe that the latter is responsible for the observed contraction. We also observed the disappearance of the (110) peak, which can also be associated to the $Co^{2+} \rightarrow Co^{3+}$ oxidation process (thermal decomposition carried out under air) followed by its partial diffusion to the interlayer space where it can attach to the neighboring layer through a grafting process. In this case, the layered structure is partially preserved but the layers are strongly disordered (disappearance of the (110) reflection). Perez-Ramirez et al. [14] showed that when the Co–Al system is decomposed under a N_2 atmosphere, the (110) reflection remains in the X-ray pattern until complete collapse of the lamellar structure. It occurs because there is no oxidation of the Co^{2+} cations. M^{3+} migration to the interlamellar region of HT was also proposed by Bellotto et al. [25].

At about 180 °C the diffraction line (003) further decreases in intensity and shifts toward higher 2θ angles, as in the case of sample HTCu30, where the *d*-spacing shifts from 0.759 to 0.665 nm. This further supports the idea that the remaining layered structure consists only of the intermediate phase whose structure is formed by the layers connected to each other via Co^{3+} cations as proposed by Perez-Ramirez et al. [14]. Furthermore, at 180 °C the appearance of a broad and weak peak at about 36° (marked with a solid circle) is observed and it becomes sharper and more intense upon further heating. This peak was assigned to the formation of Co_3O_4 (JCPDS 42–1467) with a spinel structure. This way, the intermediate lamellar phase containing Co^{3+} in the interlamellar region would be the precursor of the mixed

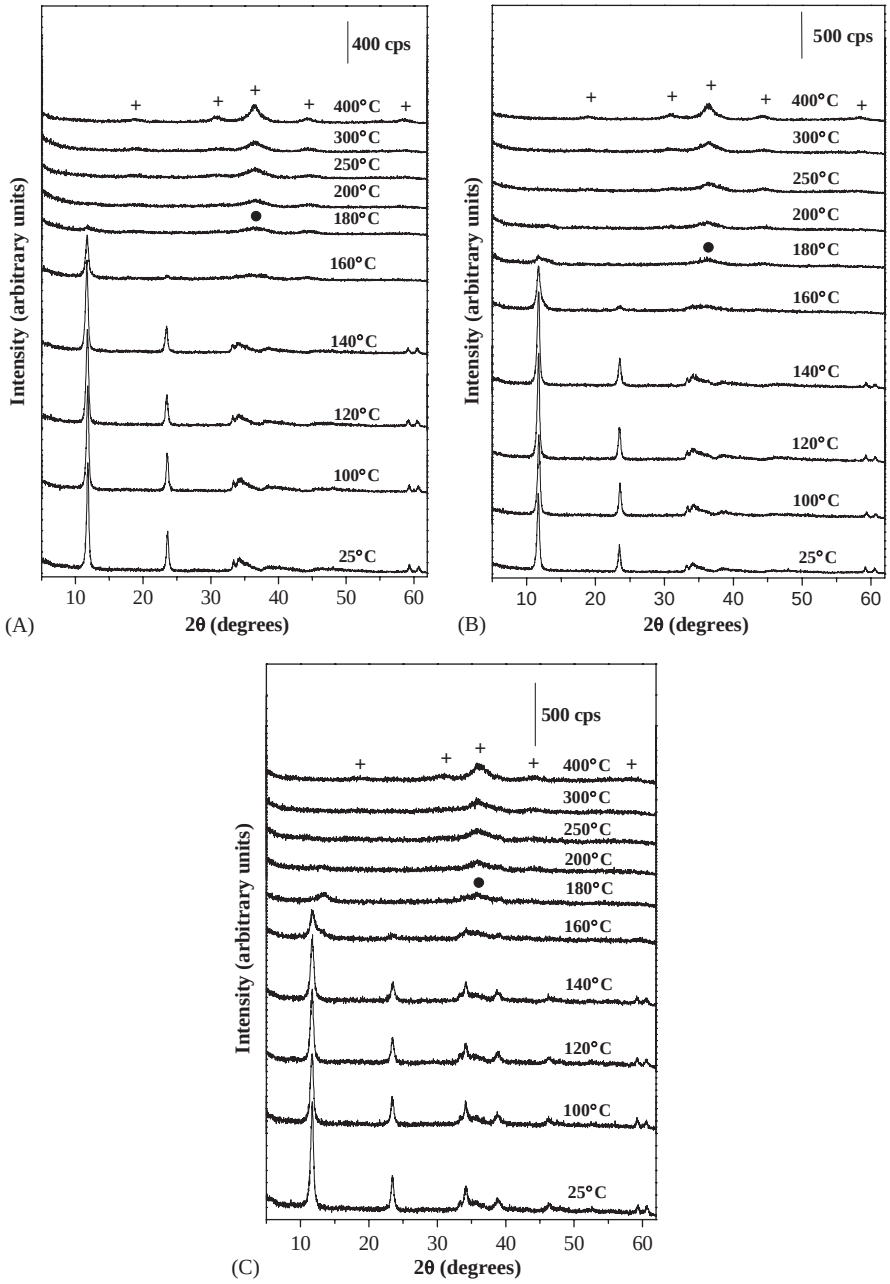

Fig. 5. In situ X-ray diffraction for (A) HTCu0, (B) HTCu10 and (C) HTCu30. The peaks related to the Co_3O_4 phase are marked with a +.

oxide Co_3O_4. The larger initial width of the peaks related to the Co_3O_4 phase indicates that other cations (Fe and Cu) could be present, thus entering the oxide structure by replacing the cobalt and forming a solid solution.

3.2.3. Mössbauer analysis

The isomer shift and quadrupolar splitting for all HT studied in the 25–300 °C temperature interval indicate that the iron is in the Fe^{3+} oxidation state with an octahedral coordination. The temperature dependence of the Mössbauer parameters is qualitatively the same for all the HT as can be seen in Fig. 6.

The isomer shift decreases as the temperature increases following the second-order Döppler shift [45]. The linewidths present a linear behavior with a very low ($d\Gamma/dT$) slope. However, the temperature dependence of the quadrupole splitting is remarkable. It increases as the temperature increases but there is a step-like feature superimposed on the linear behavior in the 140–220 °C temperature range. The higher values of quadrupolar splitting indicate an increasing degree of disorder at the Fe^{3+} site. The temperature range where the local order is lowered coincides with the structural disorder observed in the X-ray studies and in the thermal measurements. Furthermore, the magnitude of

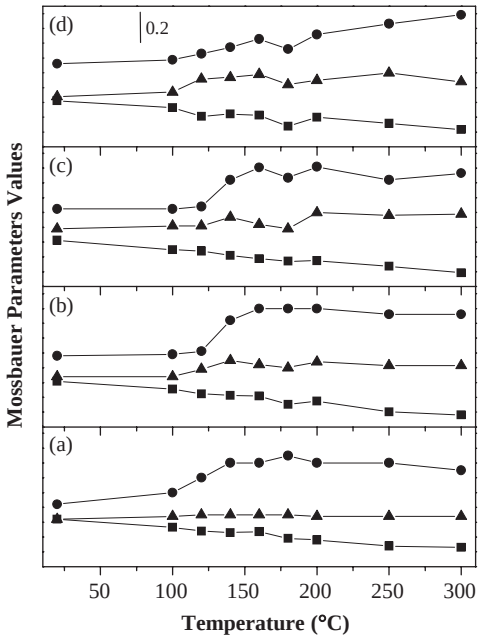

Fig. 6. The Mössbauer parameters Isomer Shift (solid square), Quadrupole Splitting (solid circle) and Linewidth (solid triangle), as a function of Cu concentration for (a) HTCu0, (b) HTCu10, (c) HTCu30, and (d) HTCu50, respectively.

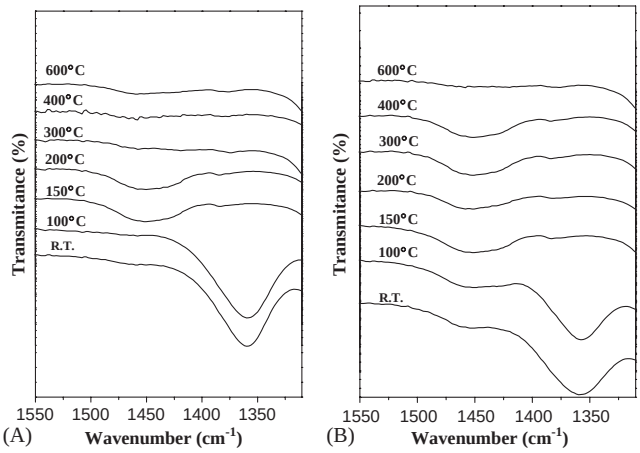

Fig. 7. FTIR for samples HTCu10 (a) and HTCu30 (b) heated at different temperatures.

the step-like feature clearly decreases as the Cu content increases. This is understood based on the structural order of the samples at room temperature. The X-ray patterns of the as prepared samples indicate that Cu-rich samples are more disordered. The maximum values observed in the quadrupolar splitting vs. temperature plots fall in the 0.7–0.8 mm/s range. Fig. 3B shows that the quadrupolar splitting systematically increases from 0.42 to 0.56 for samples from HTCu0 to HTCu50. Thus, the higher the starting quadrupolar splitting the less pronounced is the step-like feature, because it is limited to 0.8 as the highest degree of disorder observed in our samples.

3.2.4. Infrared spectroscopy

The infrared spectra of the HTCu10 and HTCu30 samples thermally treated at different temperatures are shown in Fig. 7. The analysis of the 1550–1300 cm^{-1} wavenumber region allows probing the behavior of the interlamellar anions under thermal heating (see experimental section).

From room temperature up to 100 °C the FTIR spectra do not exhibit any significative changes. The band at 1357 cm^{-1} (attributed to the asymmetric stretching (υ_3) of the carbonate) remains practically unaltered. However, by further increasing the temperature to 150 °C, this mode shifts to 1450 cm^{-1} for both HTCu10 (Fig. 7A) and HTCu30 (Fig. 7B) and its linewidth (intensity) is larger (smaller) when compared with lower temperature spectra. This change may be related to a new arrangement of the anion in the interlayer space as a consequence of the release of interlamellar water. TG measurements indicated that at 150 °C the HTCu10 (HTCu30) loses 11.2 (12.2%) of its initial weight, thus supporting the assignment that interlamellar water has been released. Furthermore, the XRD showed that the layered structure was not completely destructed. Some authors have observed this rearrangement of carbonate anions during thermal annealing, and, in general, it happens along with the anionic grafting [28,44]. However, changes of carbonate in the chemical environment of these samples cannot be attributed to the grafting process because the XRD, in this temperature range, clearly shows that the c parameter does not decrease, as expected when a grafting process occurs. Besides, we have not observed the splitting of the carbonate modes, which is also characteristic of the grafting process [28,44]. A metastable state during the decomposition process seems to be the most reasonable situation for these samples [46].

The band associated to CO_3^{2-}, located at 1450 cm^{-1}, is not observed for HTCu10 when this sample is heated at 300 °C (see Fig. 7A) whereas, for HTCu30 (Fig. 7B), it can be observed up to the annealing temperature of 400 °C. This difference in thermal behavior reflects the role of the Cu content on the layers. Thus, for Cu-rich samples there is the formation of a phase containing carbonate which is stable at high temperatures. The TG scans for high Cu concentration samples (Fig. 4B) clearly show a weight loss in the temperature interval 430–550 °C (approximately 1.5%) that should be associated to the release of carbonate from the oxi-carbonate phase. Such a phase is amorphous since, in the X-ray pattern recorded at 400 °C, only diffraction peaks associated with Co_3O_4 phases are observed. Velu et al. [26] and Kannan et al. [27] have also studied Cu-rich

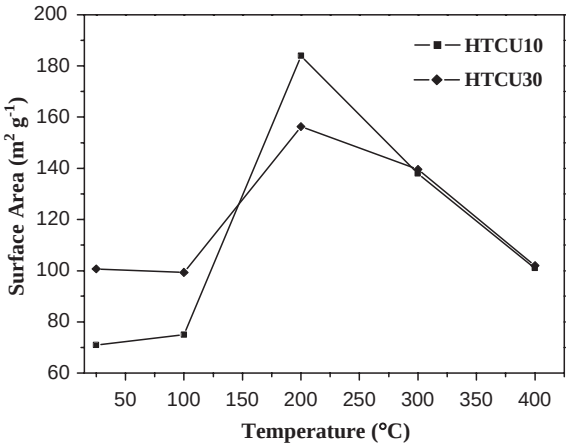

Fig. 8. Variation of specific surface area for samples HTCu10 and HTCu30 calcined at different temperatures.

ternary HT (the trivalent cation was Al^{3+}). Their study pointed out the formation of the $Cu_x(M_y)O_z(CO_3)_m$ oxi-carbonate phase during thermal annealing. Thus, the carbonate-containing phase formed in the Cu-rich samples may be of a similar nature. However, the decomposition temperature of this Cu-rich oxi-carbonate phase for CuM (M = Co, Mg, Ni and Mn) Al is higher than that which we observed for Co–Cu–Fe HT, probably due to the different Cu^{2+} content in the brucite-like sheets.

3.2.5. Specific surface area

We also carried out specific surface area measurements of the samples obtained from the thermal decomposition process of HT. The results for both HTCu10 and HTCu30 as a function of thermal treatment temperature are shown in Fig. 8.

Both samples exhibit similar temperature dependence for the surface area data. The as prepared Co–Cu–Fe present high values of surface area and this parameter exhibits a maximum value for the samples treated at 200 °C. Such behavior is due to the formation of pores when the water molecules and carbonate anions are released and to the formation of the intermediate amorphous phase. This assumption is corroborated by the in situ X-ray measurements. The sample with lower Cu content exhibits a higher surface area, thus suggesting that the presence of the oxi-carbonate prevents an increase of surface area. For temperatures higher than 200 °C, both samples present a decrease in the specific surface area. This is attributed to the onset of the crystallization of isolated phases such as Co_3O_4 and the subsequent increase of crystallite size when the temperature increases. This fact is shown in the X-ray diffractogram (Fig. 5), where the diffraction peak at 36° gains intensity and becomes narrower.

4. Conclusions

The structural and thermal properties of Co–Cu–Fe carbonate HT were studied. Since it was not possible to obtain the Cu–Fe double hydroxide, we observed that the presence of Co^{2+} is fundamental for getting the layered double hydroxide structures containing Cu^{2+} and Fe^{3+}. This effect is attributted to the strong Jahn–Teller effect that Cu^{2+} (d^9 configuration) experiences, thus introducing strong distortions in the layers that cannot be accomodated by the layers at higher concentrations. When the Cu/Co molar ratio is higher than 1, segregation of Cu-rich phases such as $Cu(OH)_2$ and CuO is observed.

Both in-situ X-ray diffraction and Mössbauer spectroscopy measurements allowed a deeper understanding of the step-by-step thermal decomposition. The results clearly indicate an increasing disorder in the brucite-like layers when the temperature increases. The $Co^{2+} \rightarrow Co^{3+}$ oxidation along with the partial migration of Co^{3+} cations to the interlayer region is discussed as a possible mechanism for the observed disorder in the layers. This process leads to the formation of a metastable compound whose structure is still layered, as unveiled by the X-ray pattern. Such an intermediate compound could be the precursor of the Co_3O_4 phase.

The interlayer space was investigated through the FTIR spectra of the interlamellar anions. By analyzing the CO_3^{2-} modes, we have observed that, for the Cu-rich HT, there is a phase that still contains carbonate even for samples treated at temperatures higher than 400 °C. This phase is an oxi-carbonate and may be associated with the high Cu content since it has not been observed for HT with low Cu (0 and 10%) concentrations. The total removal of carbonate from the solids were obtained only at temperatures higher than 550 °C. Furthermore, we have observed a metal-oxygen vibration at 350 cm^{-1} that is a spectral signature of the HT phase.

The specific surface area increases up to 200 °C where both intermediate and amorphous oxides are formed. The surface areas systematically decrease when crystallization of Co_3O_4 starts and further decrease upon increasing the temperature, as a consequence of crystallite size increments.

Acknowledgments

AHI, OPF and DXG acknowledge financial support from the Brazilian agency CNPq. AGSF acknowledge financial support from CAPES (PRODOC grant 22001018). This is a contribution of the Millennium Institute of Complex Materials.

References

[1] F. Cavani, F. Trifirò, A. Vaccari, Catal. Today 11 (1991) 173.
[2] A. de Roy, C. Forano, K. El Malki, J.B. Besse, in: M.L. Occelli, H. Robson (Eds.), Expanded Clays and Other Microporous Solids, Synthesis of Microporous Materials, van Nostrand Reinhold, New York, 1992, p. 108 (chapter 7).
[3] V. Rives, M. A Ulibarri, Coord. Chem. Rev. 181 (1999) 61.
[4] F. Triforò, A. Vaccari, in: J.L. Atwood, J.E.D. Davies, D.D. MacNicol, F. Vögtle, J.-M. Lehn, G. Alberti, T. Bein (Eds.), Comprehensive Supramolecular Chemistry, Vol. 7, Pergamon-Elsevier Science, Oxford, 1996, p. 251.
[5] A.I. Khan, D. O'Hare, J. Mater. Chem. 12 (2002) 3191.
[6] F.M. Vichi, O.L. Alves, J. Mater. Chem. 7 (1997) 1631.
[7] O.P. Ferreira, O.L. Alves, Brazilian Patent, PI 0200354-6, 2002.
[8] N.K. Lazaridis, T.A. Pandi, K.A. Matis, Ind. Eng. Chem. Res. 43 (2004) 2209.
[9] A. Vaccari, Appl. Clay Sci. 14 (1999) 161.
[10] F.O. Figueras, Top. Catal. 29 (2004) 189.
[11] A.I. Khan, L. Lei, A.J. Norquist, D. O'Hare, Chem. Commun. 22 (2001) 2342.
[12] V. Ambrogi, G. Fardella, G. Grandolini, L. Perioli, Int. J. Pharm. 220 (2001) 23.
[13] V. Rives, Mater. Chem. Phys. 75 (2002) 19.
[14] J. Pérez-Ramírez, G. Mul, F. Kapteijn, J.A. Moulijn, J. Mater. Chem. 11 (2001) 821.
[15] V. Rives, A. Dubey, S. Kannan, Phys. Chem. Chem. Phys. 3 (2001) 4826.
[16] H.B. Friedrich, F. Khan, N. Singh, M. Staden, Synlett 6 (2001) 869.
[17] S. Velu, K. Suzuki, M.P. Kapoor, F. Ohashi, T. Osaki, Appl. Catal. A 213 (2001) 47.
[18] A. Alejandre, F. Medina, X. Rodrigues, P. Salagre, Y. Cesteros, J.E. Sueiras, Appl. Catal. B 30 (2001) 195.
[19] R. Unnikrishnan, S. Narayanan, Ind. Eng. Chem. Res. 26 (1987) 173.
[20] A.A. Khassin, T.M. Yurieva, G.N. Kustova, I.S. Itenberg, M.P. Demeshkina, T.A. Kriger, L.M. Plyasova, G.K. Chermashentseva, V.N. Parmon, J. Molec. Catal. A 168 (2001) 193.
[21] S.R. Segal, K.B. Anderson, K.A. Carrado, C.L. Marshall, Appl. Catal. A 231 (2002) 215.
[22] S. Kannan, C.S. Swamy, Catal. Today 53 (1999) 725.
[23] A.E. Palomares, J.M. Lopez-Nieto, F.J. Lazaro, A. Lopez, A. Corma, Appl. Catal. B 20 (1999) 257.
[24] F. Márquez, A.E. Palomares, F. Rey, A. Corma, J. Mater. Chem. 11 (2001) 1675.
[25] M. Bellotto, B. Rebours, O. Clause, J. Lynch, D. Bazin, E. Elkaïm, J. Phys. Chem. 100 (1996) 8535.
[26] S. Velu, C.S. Swamy, J. Mater. Sci. Lett. 15 (1996) 1674.
[27] S. Kannan, V. Rives, H. Knözinger, J. Solid State Chem. 177 (2004) 319.
[28] O.P. Ferreira, O.L. Alves, D.X. Gouveia, A.G. Souza Filho, J.A.C. de Paiva, J. Mendes Filho, J. Solid State Chem. 177 (2004) 3058.
[29] P. Porta, S. Morpurgo, I. Pettiti, J. Solid State Chem. 121 (1996) 372.
[30] J. Perez-Ramirez, G. Mul, J.A. Moulijn, Vib. Spectrosc. 27 (2001) 75.
[31] M. del Arco, R. Trujillano, V. Rives, J. Mater. Chem. 8 (1998) 761.
[32] H.C. Zeng, Z.P. Xu, M. Qian, Chem. Mater. 10 (1998) 2277.
[33] E. Uzunova, D. Klissurski, I. Mitov, P. Stefanov, Chem. Mater. 5 (1993) 576.
[34] H.C.B. Hansen, C.B. Koch, R.M. Taylor, J. Solid State Chem. 113 (1994) 46.
[35] Y. Cudennec, A. Lecerf, Solid State Sci. 5 (2003) 1471.
[36] M. Vucelic, W. Jones, G.D. Moggridge, Clays Clay Miner. 45 (1997) 803.
[37] F. Leroux, E.M. Moujahid, H. Roussel, A.M. Flank, V. Briois, J.P. Besse, Clays Clay Miner. 50 (2002) 254.
[38] V. Rives, S. Kannan, J. Mater. Chem. 10 (2000) 489.
[39] F.M. Labajos, V. Rives, M.A. Ulibarri, J. Mater. Sci. 27 (1992) 1546.
[40] M.J. Hernandez-Moreno, M.A. Ulibarri, J.L. Rendom, C.J. Serna, Phys. Chem. Miner. 12 (1985) 34.
[41] B. Weckler, H.D. Lutz, Eur. J. Solid State Inorg. Chem. 35 (1998) 531.
[42] J. Danon, In Lectures on the Mössbauer Effect, Gordon and Breach, Science Publishers, New York, 1968.
[43] T. Stanimirova, I. Vergilov, G. Kirov, N. Petrova, J. Mater. Sci. 34 (1999) 4153.
[44] C. Vaysse, L. Guerlou-Demourgues, C. Delmas, Inorg. Chem. 41 (2002) 6905.
[45] U. Gonser, In Mössbauer Spectroscopy, Chapman & Hall, London, 1971.
[46] I. Melian-Cabrera, M.L. Granados, J.L.G. Fierro, Phys. Chem. Chem. Phys. 4 (2002) 3122.